ORIGINAL ARTICLE

Open Access

Switching Frequency Improvement of a High Speed on/off Valve Based on Pre-excitation Control Algorithm

Qi Zhong[1,2,3]* , Xiaotian Li[1,3], Yongxin Mao[1,3], Enguang Xu[1,3], Tiwei Jia[1,3], Yanbiao Li[1,3] and Huayong Yang[2]

Abstract

The high-speed on/off valve (HSV) serves as the fundamental component responsible for generating discrete fluids within digital hydraulic systems. As the switching frequency of the HSV increases, the properties of the generated discrete fluid approach those of continuous fluids. Therefore, a higher frequency response characteristic of HSV is the key to ensure the control accuracy of digital hydraulic systems. However, the current research mainly focuses on its dynamic performance, but neglect its FRC. This paper presents a theoretical analysis demonstrating that the FRC of the HSV can be enhanced by minimizing its switching time. The maximum switching frequency (MSF) is mainly determined by opening dynamic performance when HSV operates with low switching duty ratio (SDR), whereas the closing dynamic performance limits the MSF when HSV operates with high SDR. Building upon these findings, the pre-excitation control algorithm (PECA) is proposed to reduce the switching time of the HSV, and consequently enhance its FRC. Experimental results demonstrate that PECA shortens the opening delay time of HSV by 1.12 ms, the closing delay time by 2.54 ms, and the closing moving time by 0.47 ms in comparison to the existing advanced control algorithms. As a result, a larger MSF of 417 Hz and a wider controllable SDR range from 20% to 70% were achieved at a switching frequency of 250 Hz. Thus, the proposed PFCA in this paper has been verified as an effective and promising approach for enhancing the control performance of digital hydraulic systems.

Keywords High speed on/off valve, Switching frequency, Pre-excitation, Dynamic performance, Switching duty ratio

1 Introduction

The digital hydraulic system is able to achieve the control effect of continuous fluids by utilizing discrete fluids [1, 2]. High speed on/off valve (HSV) is the core component for generating discrete fluids by switching behavior [3, 4]. Due to the HSV's binary operational states of 'ON' and 'OFF', the average output flow can be changed by adjusting its switching duty ratio (SDR). Consequently, as the switching frequency of the HSV increases, the characteristics of the discrete fluid it generates approach those of continuous fluids [5]. This leads to improved response speed and enhanced control accuracy within the digital hydraulic system. Therefore, enhancing the switching frequency of HSV holds great significance in the realm of digital hydraulics.

Numerous studies have been conducted to improve the dynamic performance of HSV, aiming to accelerate its switching process [6, 7]. Optimization the control algorithm has been proved as a highly effective and economical approach to enhance the dynamic performance for the existing HSVs [8, 9]. Despite the strong feasibility of the traditional single-voltage control algorithm (SCA)

*Correspondence:
Qi Zhong
zhongqi@zjut.edu.cn
[1] College of Mechanical Engineering, Zhejiang University of Technology, Hangzhou 310023, China
[2] State Key Laboratory of Fluid Power and Mechatronic Systems, Zhejiang University, Hangzhou 310027, China
[3] Key Laboratory of Special Purpose Equipment and Advanced Processing Technology, Ministry of Education and Zhejiang Province, Zhejiang University of Technology, Hangzhou 310023, China

and the double-voltage control algorithm [10], they fall short of meeting expectations in terms of enhancing the dynamic performance of HSV. Therefore, three-voltage control algorithm (TCA) was proposed to speed up the switching process of the HSV. Based on this algorithm, Lee [11] designed a three-voltage driving circuit, which reduced the holding current during maintenance stage, and finally shortened the closing delay time. However, the excitation time of each voltage in this circuit needs to be preset by calculations and tests, and cannot be adjusted in real-time. To address this issue, Zhong et al. [12] proposed an intelligent pulse width modulation (PWM) control algorithm that enables adaptive switching of driving voltages based on current feedback, thereby achieving an accelerated dynamic performance of the HSV. Building upon this foundation, an additional self-correcting PWM control method was further proposed to improve and preserve the HSVs' original dynamic performance when subjected to varying pressures [13]. A compound PWM control algorithm which consists of reference PWM, excitation PWM, high frequency PWM and reverse PWM was presented to improve the dynamic performance [14]. The preceding work considerably optimized the dynamic performance of HSV but neglected the excessive coil current rise, which will lead to higher energy loss and worse reliability [15, 16]. Therefore, a comprehensive investigation was conducted into the holding current of TCA, leading to the conclusion that an optimal holding current can concurrently enhance dynamic performance and energy efficiency [17], thereby extending the service life [18, 19]. The effect of boost voltage was also investigated to explore the correlation between dynamic performance and power losses [20]. Breidi et al. [21] explored the impact of peak-and-hold technology and reverse current, and proposed an enhanced TCA that reduced the opening and closing times of HSV by 80% and 64%, respectively, in comparison to SCA.

The aforementioned TCAs optimized the initial closing current by peak-and-hold technology, but neglected initial opening current optimization, resulting in minimal improvement in opening dynamic performance. In order to overcome this, Zhong et al. proposed a four-voltage control algorithm [22] that excites the HSV before the switching target, so that both initial opening and closing current can be optimized close to the critical switching currents, and a rapid response speed can be achieved. The superiority of this algorithm was also confirmed in a commercial solenoid screw-in cartridge valve [23]. Moreover, the controllable and adjustable dynamic performance of HSV were also achieved by optimizing this four-voltage control algorithm [24].

The above researches focus on the dynamic performance of HSV, but neglect its frequency response characteristic (FRC), which is a crucial feature representing the capability of the HSV to track and continuously respond to switching targets. The FRC has a significantly impact on both the dynamic and static performance of HSV-controlled system.

In order to obtain a greater FRC of the HSV, the multi-field mathematical model of the HSV is developed, and the theoretical solutions of dynamic performance were derived, and its effects on maximum switching frequency (MSF) was discussed. A pre-excitation control algorithm (PECA) is proposed to improve the FRC of HSV by speeding up its switching behaviors. Simulated and experimental results indicate that the PECA enables the HSV to achieve a greater FRC and a wider linear adjustable range of SDR, offering a practical and economic approach for expanding the applications of digital hydraulic systems requiring enhanced FRC.

2 Structure and Theoretical Analysis of HSV

2.1 Operation Principle of HSV
In this research, a conventional HSV is used as the research object, which is a two-position two-way normal closed solenoid valve, its structure is illustrated in Figure 1(a). When the coil is de-energized, the spring force turns the spool to the right side so that the HSV works in statue 'OFF', preventing the fluid from passing, as shown in Figure 1(b). Conversely, when the coil is energized, the electromagnetic force against the spring force to move the spool to the left side, so the HSV operates in statue 'ON', allowing for the fluid to pass, as shown in Figure 1(c).

2.2 Electromagnetic Characteristic Analysis
The electrical characteristic of HSV is given by:

$$U = RI + L\frac{\mathrm{d}I}{\mathrm{d}t} + I\frac{\mathrm{d}L}{\mathrm{d}t}, \tag{1}$$

where U denotes the driving voltage, R represents the equivalent resistance, I denotes the coil current and L is the equivalent inductance.

The electromagnetic force generated by the solenoid can be expressed as:

$$F_{\mathrm{m}} = \frac{\phi^2}{2\mu_{\mathrm{a}}S_{\mathrm{gap}}} = \frac{B^2 S_{\mathrm{gap}}}{2\mu_{\mathrm{a}}}, \tag{2}$$

where F_{m} is the electromagnetic force, ϕ denotes the magnetic flux, μ_{a} represents the air permeability, S_{gap} is the air gap cross-sectional area and B denotes the magnetic flux density.

The non-linear characteristic between the magnetic flux density B and magnetic field intensity H can be expressed as:
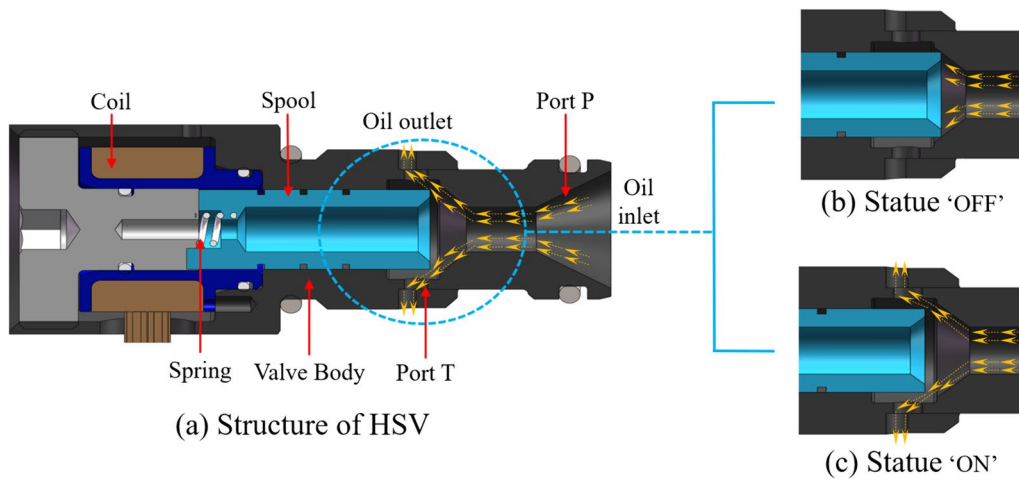
Figure 1 Structure of the HSV

$$B = f(H). \tag{3}$$

The relationship between the magnetic field intensity H and the coil current can be represented as:

$$H = \frac{IN}{L_e}, \tag{4}$$

where N is the turns of coil, L_e denotes the effective magnetic path length.

Therefore, the electromagnetic force F_m can be expressed as:

$$F_m = \frac{[f(\frac{IN}{L_e})]^2 S_{gap}}{2\mu_a}. \tag{5}$$

2.3 Switching Behavior Analysis

The kinetic equation of the HSV can be represented as:

$$m\frac{d^2x}{dt^2} = F_m - (F_t + F_s) - k\frac{dx}{dt} + P_sA - k_s(x + x_0) \pm F_f, \tag{6}$$

where m and x present the mass and displacement of spool, respectively, F_t and F_s stand for the transient hydraulic force and steady hydraulic force, respectively, k is the damping coefficient, P_s represents the supply pressure, A stands for the effective cross-sectional area of port P, k_s denotes the elasticity coefficient of spring, x_0 stands for the compression of the spring, F_f indicates the friction force between spool and valve body, and its symbol depends on the direction of the force, the same as the electromagnetic force is "+", the opposite is "−".

The transient hydraulic force F_t and the steady hydraulic force F_s can be expressed as:

$$F_s = 2C_vC_dA_0\Delta P\cos\theta, \tag{7}$$

$$F_t = 2C_d\omega L_d\sqrt{2\rho\Delta P}\frac{dx}{dt}, \tag{8}$$

where C_v and C_d stand for the fluid velocity coefficient and flow coefficient, respectively, A_0 is the open area of orifice, ΔP denotes the pressure difference between port P and port T, θ indicates the flow angle, ω stands for the area gradient, L_d is the oil damping length, ρ denotes the density of oil.

At the moment of critical switching state, the velocity and acceleration of the spool are both zero, so the critical opening electromagnetic force F_{on} and the critical closing electromagnetic force F_{off} of the HSV can be respectively expressed as:

$$F_{on} = k_sx_0 + F_f - P_sA, \tag{9}$$

$$F_{off} = F_s - P_sA + k_s(x_0 + d_{gap}) - F_f, \tag{10}$$

where d_{gap} represents the stroke of the spool.

Therefore, the critical opening current I_{on} and critical closing current I_{off} of HSV can be derived as:

$$I_{on} = \frac{L_{eon}}{N}f^{-1}(\sqrt{\frac{2\mu_aF_{on}}{S_{gap}}}), \tag{11}$$

$$I_{off} = \frac{L_{eoff}}{N}f^{-1}(\sqrt{\frac{2\mu_aF_{off}}{S_{gap}}}), \tag{12}$$
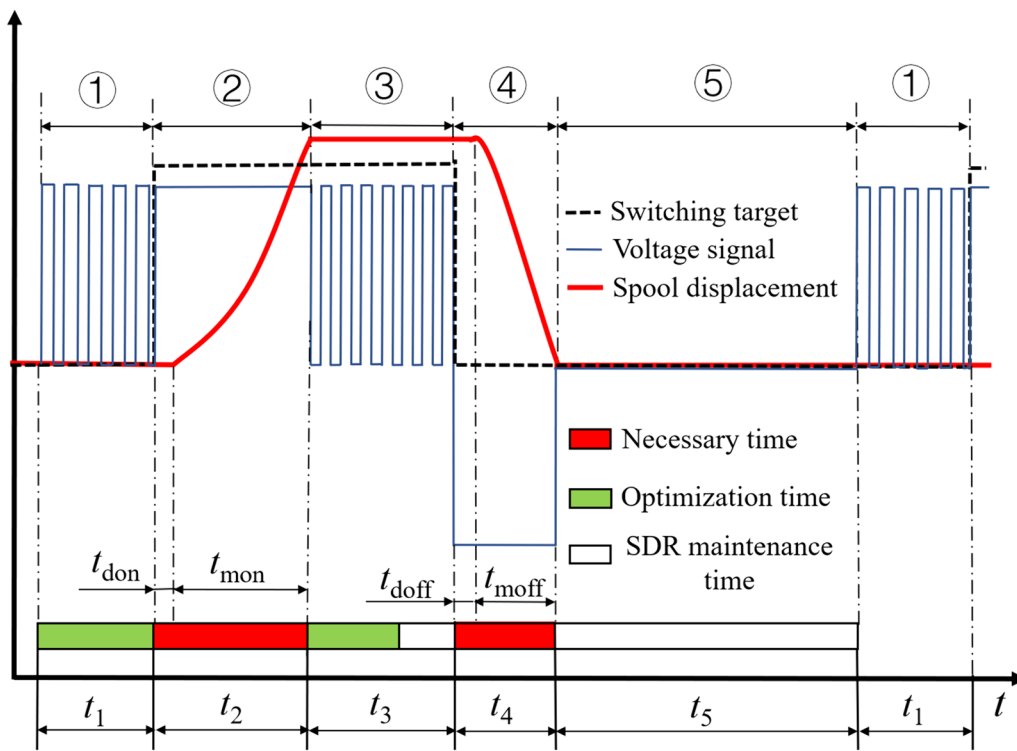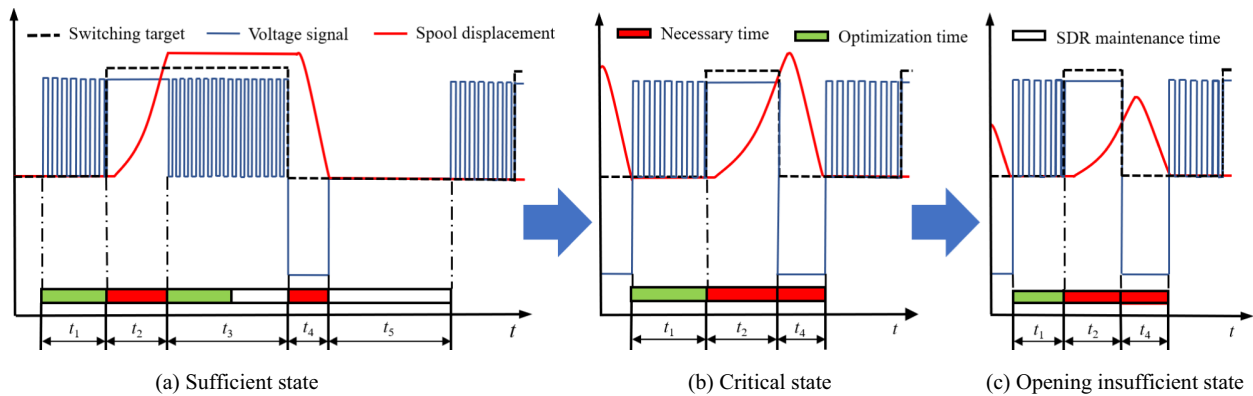
Figure 2 Operation principle of PECA

Figure 3 Switching states of HSV

where L_{eon} and L_{eoff} stand for the effective magnetic circuit length of HSV working in statue 'ON' and 'OFF', respectively.

During the switching process, the characteristic of the coil current can be represented as:

$$I = \frac{U}{R} + \left(I_i - \frac{U}{R}\right)e^{-\frac{R}{L}t}, \tag{13}$$

where I_i denotes the initial current.

The switching process is composed by opening time (subdivided into an opening delay time t_{don} and an opening moving time t_{mon}) and closing time (separated into a closing delay time t_{doff} and a closing moving time t_{moff}). The switching delay time of the HSV [8, 25] are given by:

$$t_{don} = \frac{L_{off}}{R} \ln\left(\frac{U_{on} - I_i R}{U_{on} - I_{on}R}\right), \tag{14}$$

$$t_{\text{doff}} = \frac{L_{\text{on}}}{R} \ln \left(\frac{I_i R - U_{\text{off}}}{I_{\text{off}} R - U_{\text{off}}} \right), \tag{15}$$

where L_{on} and L_{off} are the equivalent inductance of HSV working in statue 'ON' and 'OFF', individually. U_{on} and U_{off} stand for the opening voltage and closing voltage, respectively.

The dynamic behaviors of the spool in moving stages can be expressed as:

$$d_{\text{gap}} = \int_0^{t_{\text{mon}}} \left(\int_0^{\tau} \frac{F_m - (F_t + F_s) - k\frac{dx}{dt} + P_s A - k_s(x + x_0) - F_f}{m} dt \right) d\tau, \tag{16}$$

$$-d_{\text{gap}} = \int_0^{t_{\text{moff}}} \left(\int_0^{\tau} \frac{F_m - (F_t + F_s) - k\frac{dx}{dt} + P_s A - k_s(x + x_0) + F_f}{m} dt \right) d\tau. \tag{17}$$

2.4 FRC Analysis

To optimize the dynamic performance of HSV for better FRC, the PECA is presented, which consisting of five stages, they are: Pre-opening stage ①, opening stage ②, pre-closing stage ③, closing stage ④ and maintaining closed stage ⑤, respectively. The durations of these stages are denoted as t_1 to t_5, as shown in Figure 2.

There is an inverse relationship between the switching frequency f and the cycle time t_c and, in general, is divided into target-on time t_{on} and target-off time t_{off}.

$$f = \frac{1}{t_c} = \frac{1}{t_{\text{on}} + t_{\text{off}}}, \tag{18}$$

$$t_{\text{on}} = t_2 + t_3 = t_{\text{don}} + t_{\text{mon}} + t_3, \tag{19}$$

$$t_{\text{off}} = t_1 + t_4 + t_5 = t_1 + t_{\text{doff}} + t_{\text{moff}} + t_5. \tag{20}$$

So that the SDR can be represented as:

$$\alpha = \frac{t_{\text{on}}}{t_c}. \tag{21}$$

According to different functions, each cycle time is separated into necessary time, optimization time and SDR maintenance time, respectively. The necessary time refers to the minimum duration required to achieve complete switching of the HSV, encompassing the time of the opening stage ② and closing stage ④. The optimizing time is to shorten the switching delay time by increasing or decreasing the initial current in advance. Once the coil current reaches a preset value around the critical switching current, the optimization impact of the delay time becomes fully apparent. The SDR maintenance time is employed to ensure that the switching statues of HSV

aligns with the preset switching target, and it does not contribute to FRC optimization.

The MSF is a specific manifestation of FRC, which is represented by the critical value of the switching frequency under different SDRs. When it is exceeded, HSV will not be able to fully switch. As depicted in Figure 3(a), the HSV operates in a sufficient state, allowing ample time for optimizing its dynamic performance. When the switching frequency of the HSV increases with a fixed SDR, the SDR maintenance time initially decreases. Subsequently, the optimization time also decreases once the SDR maintenance time is exhausted. Eventually, only the necessary time for the complete switching of the HSV is left in the opening stage or the closing stage or both. The opening limit is taken as an example, its critical state of operation is illustrated in Figure 3(b). Then the frequency is the MSF of HSV under the current SDR. Furthermore, any further reduction in cycle time would result in the target-on or target-off time being insufficient, thereby preventing the HSV from fully opening or closing. This insufficient state of operation is depicted in Figure 3(c).

The MSF fluctuates depending on the specific SDR. Based on the above theoretical analysis, it is evident that the key factor influencing the MSF is the necessary time. However, it is important to note that the target-on and target-off time typically do not decrease to the necessary time simultaneously. Therefore, the analysis of MSF in HSV can be divided into three situations: Small SDR (where the target-on time firstly reaches the necessary time), large SDR (where the target-off time firstly reaches the necessary time) and critical SDR (where both of them reach the necessary time simultaneously).

When HSV operates under small SDR, the target-on time first reaches its minimum, which is expressed as $t_{\text{on-min}}$, as the frequency increases. The minimum target-on time can exactly ensure the HSV fully open, as shown in Figure 4.

In the critical state with ample target-off time, the total time of opening delay and opening moving exceeds the target-on time. The reason is that the final current during the opening stage ② is higher than the critical closing current, causing the HSV to not close immediately upon entering the closing stage ④, but instead continues to open. Therefore, a short necessary time of opening stage ② can meet
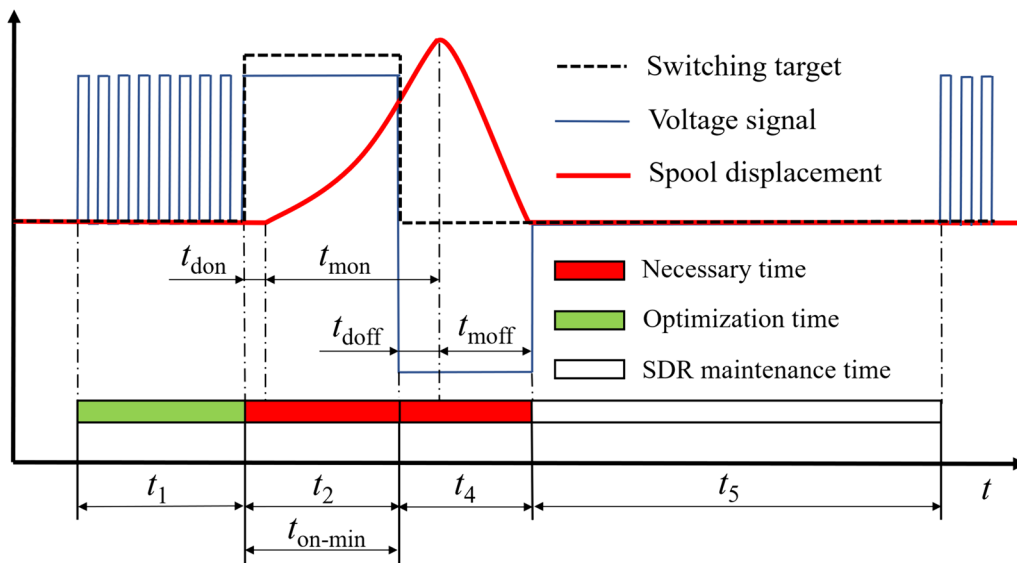
Figure 4 Minimum opening time at a small SDR

the requirement of full HSV opening. Due to the moment of HSV full opening is within the target-off time, followed by the closing process immediately, the closing delay time is completely included in the opening moving time. Thus, the minimum target-on time and its relationship to MSF can be expressed as:

$$t_{\text{on-min}} = t_{\text{don}} + t_{\text{mon}} - t_{\text{doff}}, \tag{22}$$

$$f_{\text{m}} = \frac{\alpha}{t_{\text{on-min}}}. \tag{23}$$

However, when HSV operates under large SDR, the target-off time first reaches its minimum, as expressed as $t_{\text{off-min}}$, which is critically enough for HSV to be completely closed. Therefore, the MSF of HSV is determined by the minimum target-off time, and the principle is shown in Figure 5.
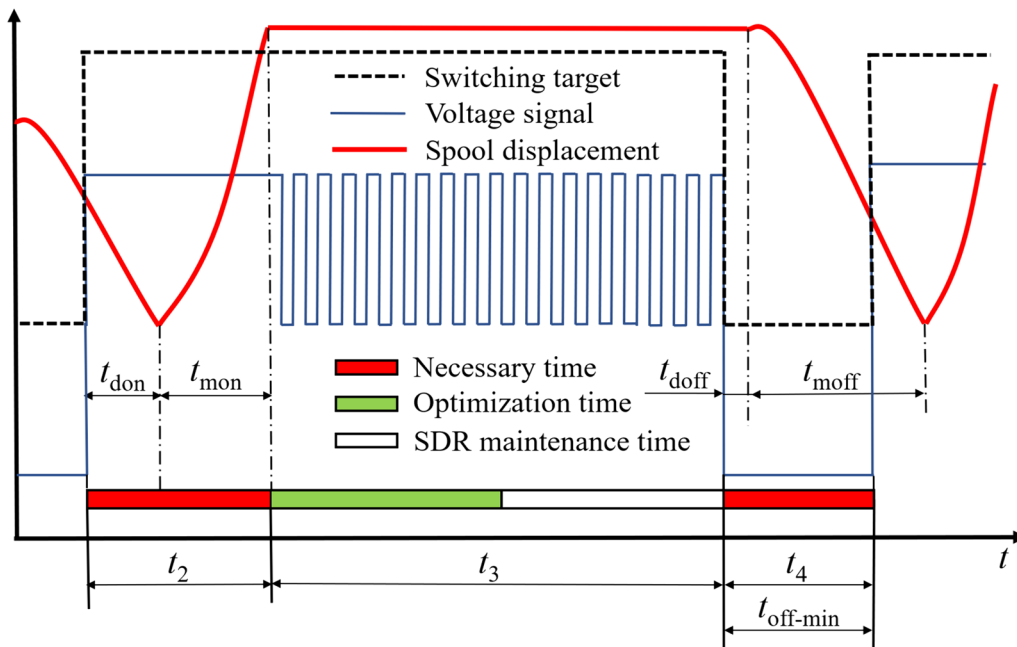

Figure 5 Minimum closing time at a large SDR

It is obvious that the sum of closing delay time and closing moving time exceeds the target-off time. This is attributed to the fact that the final current during the closing stage ④ is lower than the opening current. As a result, the HSV does not open immediately after the opening target arrives for the next cycle, but instead continues to close. Therefore, less necessary time of the closing stage ④ also achieves the closing of HSV. It is completely closed within the target-on time of the next cycle, and the minimum target-off time can be expressed as:

$$t_{\text{off-min}} = t_{\text{doff}} + t_{\text{moff}} - t_{\text{don}}. \tag{24}$$

The relationship of minimum target-off time and MSF is shown as:

$$f_{\text{m}} = \frac{1 - \alpha}{t_{\text{off-min}}}. \tag{25}$$

In particular, when both the target-on and target-off time are reduced to the necessary time simultaneously, the MSF reaches its limit value f_{lim}, which can be represented by Eq. (26):

$$f_{\text{lim}} = \frac{1}{t_{\text{on-min}} + t_{\text{off-min}}} = \frac{1}{t_{\text{mon}} + t_{\text{moff}}}, \tag{26}$$

where the I_{mon} and I_{moff} are the final current of opening moving stage and closing moving stage, individually.

Under the limit MSF, the influence of the pre-excitation stages ① and ③ decreases to the minimum. The HSV operates in a critical state where it is preparing to close immediately after opening and getting ready to open after closing, as shown in Figure 6.

Based on the above analysis, it is obvious that the necessary time for HSV is inversely proportional to its dynamic performance. Therefore, improving the dynamic performance of HSV results in smaller necessary time and higher MSF, which contributes to achieving superior FRC of the HSV.

3 Experiment Setup

3.1 Experimental Testbench Setting

The experiment testbench is shown in Figure 7(a). The voltage source provides the driving voltage to the drive module, which has been prewritten with the PECA. Due to the compact structure of the HSV, the dynamic behavior of the spool is difficult to detect using conventional displacement sensors. To address this issue, a spool displacement lead-out structure is implemented, as illustrated in Figure 7(b). The displacement of the spool is measured by a laser displacement sensor that irradiates the surface of the sheet metal. A fine needle is used to
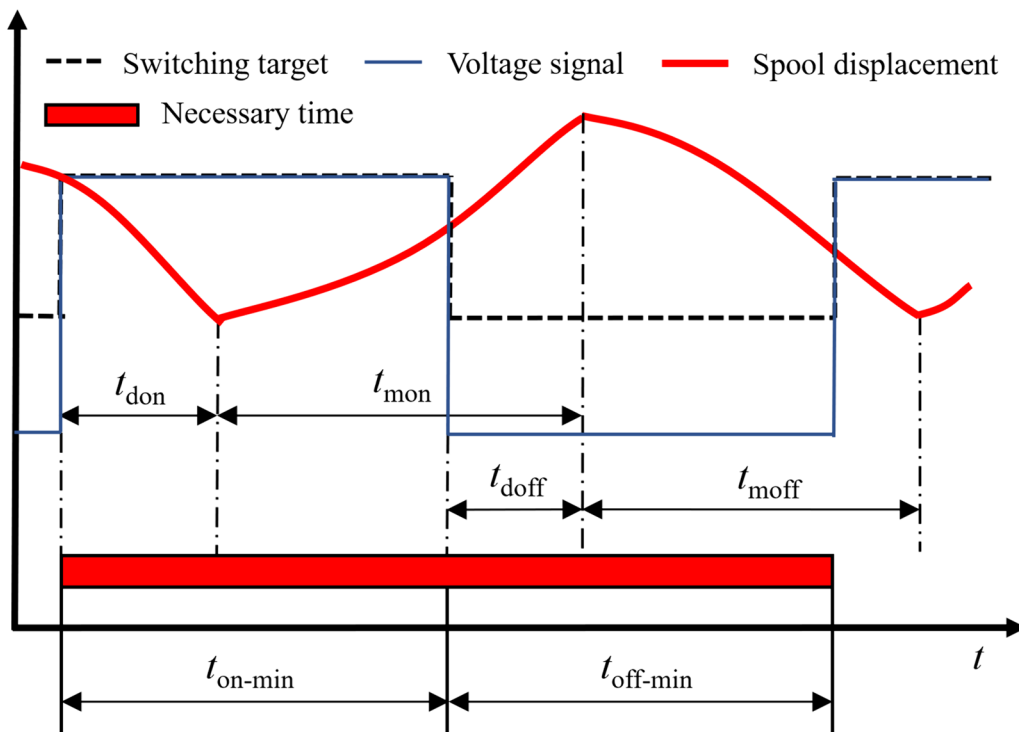

Figure 6 Limit switching state

(a) Photo of experiment testbench

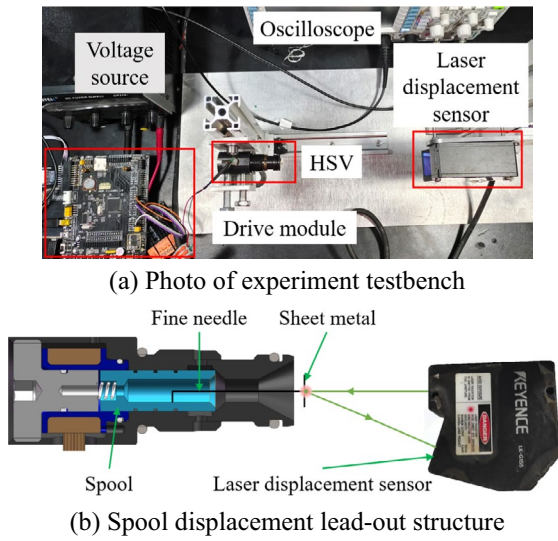(b) Spool displacement lead-out structure

Figure 7 Experimental testbench setting

connect the spool and the sheet metal, ensuring that they have the same dynamic performance. The oscilloscope is used to display the test results.

3.2 Parameter Settings

To avoid unexpected switching behavior of the HSV, the initial opening current should be smaller than the critical opening current, and the initial closing current should be larger than the critical closing current. Therefore, the range of pre-opening voltage $U_{\text{pre-on}}$ and pre-closing voltage $U_{\text{pre-off}}$ can be determined as:

$$U_{\text{pre-on}} = U\delta_{\text{pre-on}} < \frac{I_{\text{on}}R}{\left(1 - e^{-\frac{Rt_{\text{pre-on}}}{L_{\text{off}}}}\right)}, \tag{27}$$

$$U_{\text{pre-off}} = U\delta_{\text{pre-off}} > \frac{(I_{\text{off}} - I_{\text{don}}e^{-\frac{Rt_{\text{pre-off}}}{L_{\text{on}}}})R}{\left(1 - e^{-\frac{Rt_{\text{pre-off}}}{L_{\text{on}}}}\right)}, \tag{28}$$

where $\delta_{\text{pre-on}}$ and $\delta_{\text{pre-off}}$ stand for the pre-opening duty ratio and pre-closing duty ratio, respectively. $t_{\text{pre-on}}$ is the duration of the pre-opening stage ① and $t_{\text{pre-off}}$ represents the load time of the pre-closing stage ③, I_{don} denotes the final current during the opening stage ②.
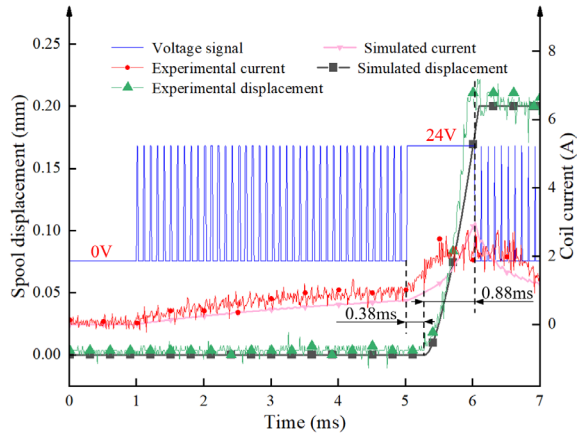
Based on theoretical analysis and experimental measurement, it can be deduced that the critical opening current of HSV is 2.1 A, while the critical closing current is 0.4 A. Consequently, the pre-opening duty ratio and pre-closing duty ratio are set at 32% and 13% respectively. The corresponding pre-opening and
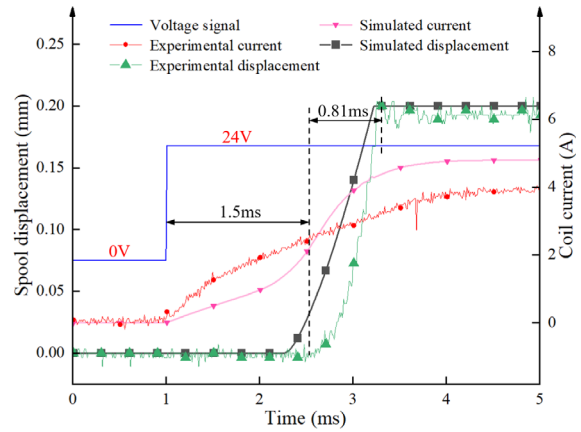
(a) SCA opening stage
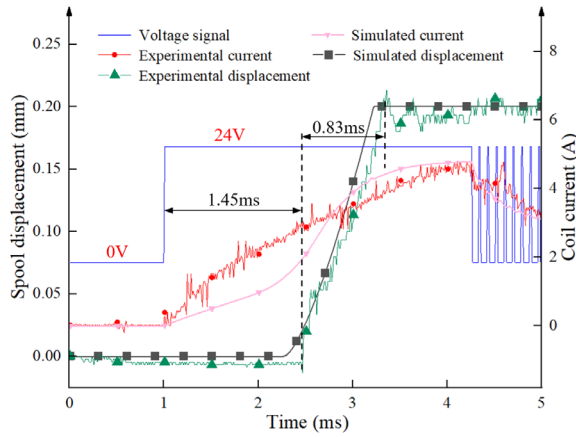
(b) TCA opening stage

(c) PECA opening stage

Figure 8 Opening dynamic performance

pre-closing voltages are equivalent as 7.68 V and 3.12 V individually.

4 Experimental Analysis of FRC

4.1 Small SDR Situation

The simulation and experimental comparison results of HSV's opening dynamic performance under three control algorithms are shown in Figure 8. It is evident that the results of dynamic performance in simulations and experiments are well-matched. Due to the same opening voltage and initial current, the opening time of HSV under SCA and TCA is similar, which is 2.31 ms and 2.28 ms, respectively. This can be observed from Figure 8(a) and (b).

The PECA proposed in this paper is beneficial to increase the initial opening current with the pre-opening voltage. When the opening target is received, the current quickly surpasses the critical value due to the excitation of the opening voltage, initiating the movement of the spool, as illustrate in Figure 8(c). Without the excitation of pre-opening voltage, the opening delay time of SCA and TCA is 1.5 ms and 1.45 ms respectively. While PECA drives, it is significantly reduced to 0.38 ms, and the opening dynamic performance is significantly improved. On the other hand, due to the same opening voltage, the opening moving time under three control algorithms is approximately equal.

A shorter opening delay time results in a reduced necessary time required for the HSV to fully open, which means that the target-on time can reach a smaller value. Eq. (23) shows that the shorter the minimum target-on time, the higher the MSF, which is verified in Figure 9.

Comparing with TCA, it is found that the MSF obtained by PECA under different SDR conditions (10% to 45%) has increased by 93 Hz on average. When the necessary time of the opening stage ② remains constant, the improvement on MSF will be linearly related to the increase of SDR, which can be represented by Eq. (29):

$$\Delta f = \left[\frac{\alpha}{(t_{\text{on-min}})_{PECA}} - \frac{\alpha}{(t_{\text{on-min}})_{TCA}} \right], \tag{29}$$

where Δf is the difference of MSF under PECA and TCA.

However, when the SDR exceeds 25%, the difference of MSF driven by TCA and PECA gradually diminish. When the SDR exceeds 45%, the time of pre-opening stage ① is severely insufficient, which greatly weakens its optimization effect. This can be attributed to the fact that as the SDR increases, it cannot guarantee sufficient time of pre-opening stage ① to optimize the initial opening current. Consequently, when the opening target arrives, the coil current fails to reach the expected optimized current, necessitating an additional delay in the opening time. Thus, the improving effect on MSF gradually weakens. As the SDR reaches about 50%, the pre-opening time is completely occupied by the closing time in the last cycle, and only the opening voltage remains to drive HSV to open. Meanwhile HSV reaches the critical state, the MSF driven by PECA is similar to that driven by TCA, and reached the limit MSF.

In addition, driven by SCA, the absence of reverse voltage during the closing stage ④ weakens the rate of current reduction, resulting in unfavorable closing dynamic performance of HSV. Therefore, the necessary time for closing stage ④ is longer than that of opening stage ②.
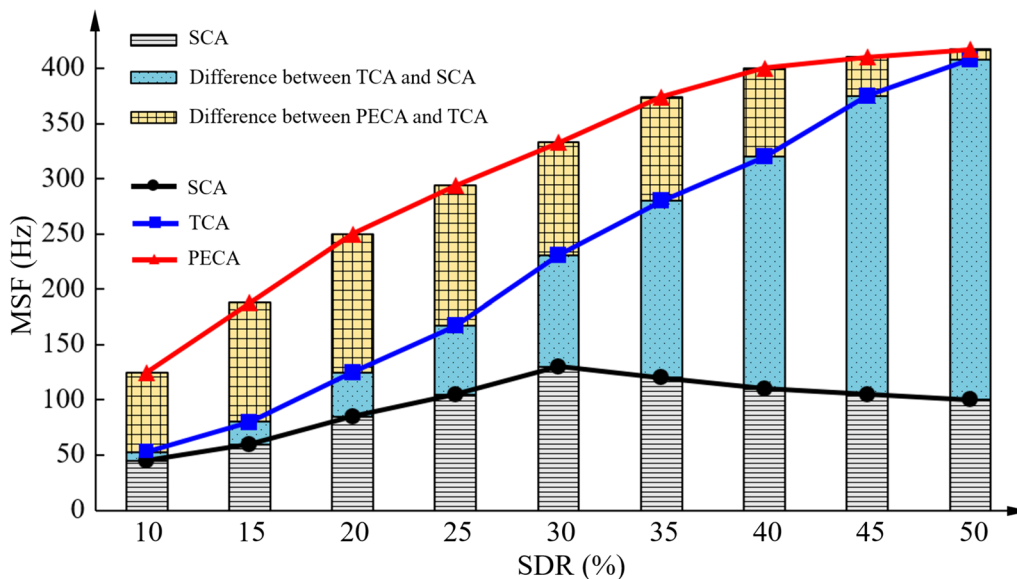

Figure 9 MSF results in small SDR situation

(a) SCA closing stage

(b) TCA closing stage
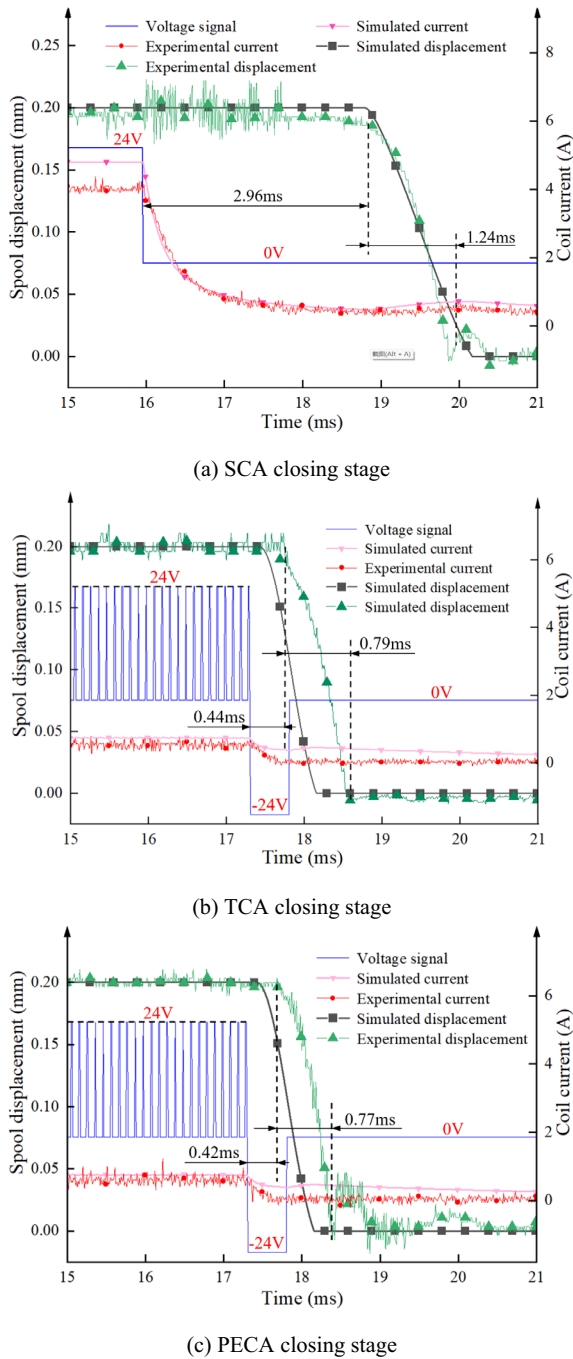

(c) PECA closing stage

Figure 10 Closing dynamic performance

When the SDR exceeds 30%, the HSV is considered to operate in a large SDR situation that is affected by the necessary time of the closing stage ④. As a result, Figure 9 shows the MSF of the HSV driven by the three Algorithms in the small SDR condition, and also the partially SCA-driven MSF in the large SDR condition.

4.2 Large SDR Situation

The comparison results of the closing dynamic performance of HSV are presented in Figure 10. Due to the effect of the pre-closing voltage under TCA-driven and PECA-driven, the initial closing current will decrease before the closing target is reached. When the time of pre-closing stage ③ is adequate, the current can be decreased to slightly above the critical closing current, effectively reducing the closing delay time. When the closing target arrives, reverse high voltage is applied to expedite the decrease in current, leading to a rapid reduction of electromagnetic force and accelerating the closing behavior of the HSV. Thus, the closing time of the HSV driven by TCA and PECA is similar due to the same closing voltage and initial current, which is 1.23 ms and 1.19 ms, respectively. However, the absence of pre-closing stage ③ and the zero voltage driving during the closing stage ④ result in suboptimal closing dynamic performance under SCA control. The closing moving time is optimized from 1.24 ms to 0.77 ms under PECA drive, when the closing delay time is decreased from 2.96 ms to 0.42 ms, comparing with that under SCA drive.

Improving the closing dynamic performance can reduce the necessary time during the closing stage ④. As shown in Eq. (25), a higher MSF can be achieved. The experimental results of MSF under TCA-driven and PECA-driven demonstrate consistent and significant improvements compared to those under SCA-driven, considering their similar closing dynamic performance, as shown in Figure 11. Additionally, it is evident that the frequency at which HSV can respond to complete switching will decrease as the SDR increases.

The results of MSF under PECA and TCA are relatively close due to the similar necessary closing time of HSV. When the closing dynamic performance of HSV remains constant, the MSF and SDR exactly satisfy a negative linear correlation. Furthermore, the relationship between the difference of MSF and SDR can be summarized as follows:

$$\Delta f = \left[\frac{1-\alpha}{(t_{\text{off-min}})_{PECA}} - \frac{1-\alpha}{(t_{\text{off-min}})_{SCA}} \right]. \tag{30}$$

However, when the SDR is in the range of 50%−60%, it is evident that there is no linear relationship driven by the PECA and TCA. The nonlinearity can be attributed to the insufficient pre-closing time as the switching frequency increases. The optimization effect of the initial closing current is weakened by the gradual decrease in pre-closing time. When the closing target arrives, the coil current fails to reach the expected optimized current. This leads to an increase in the closing delay time, which requires a longer
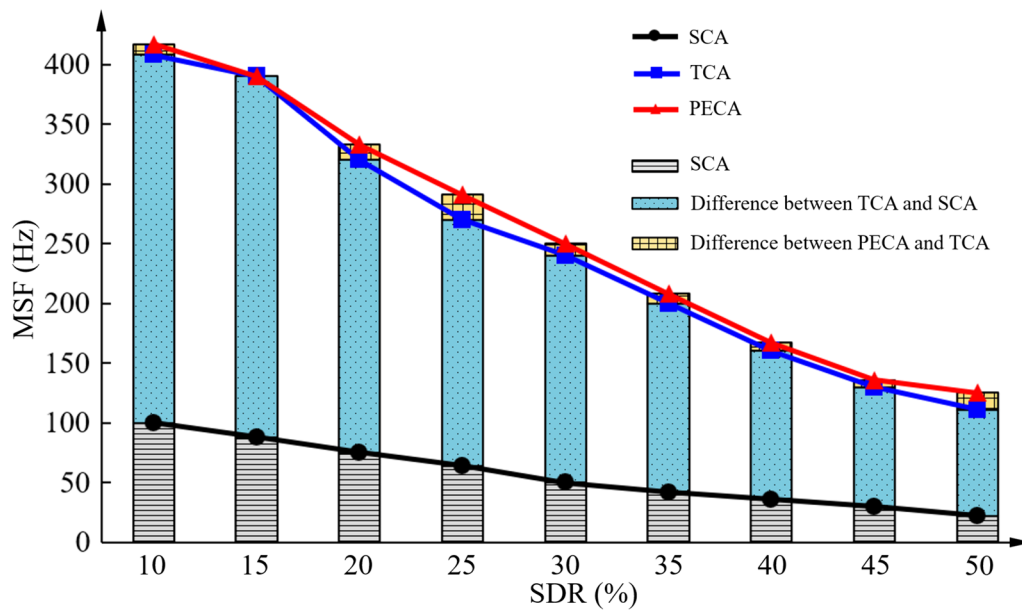
Figure 11 MSF results in large SDR situation
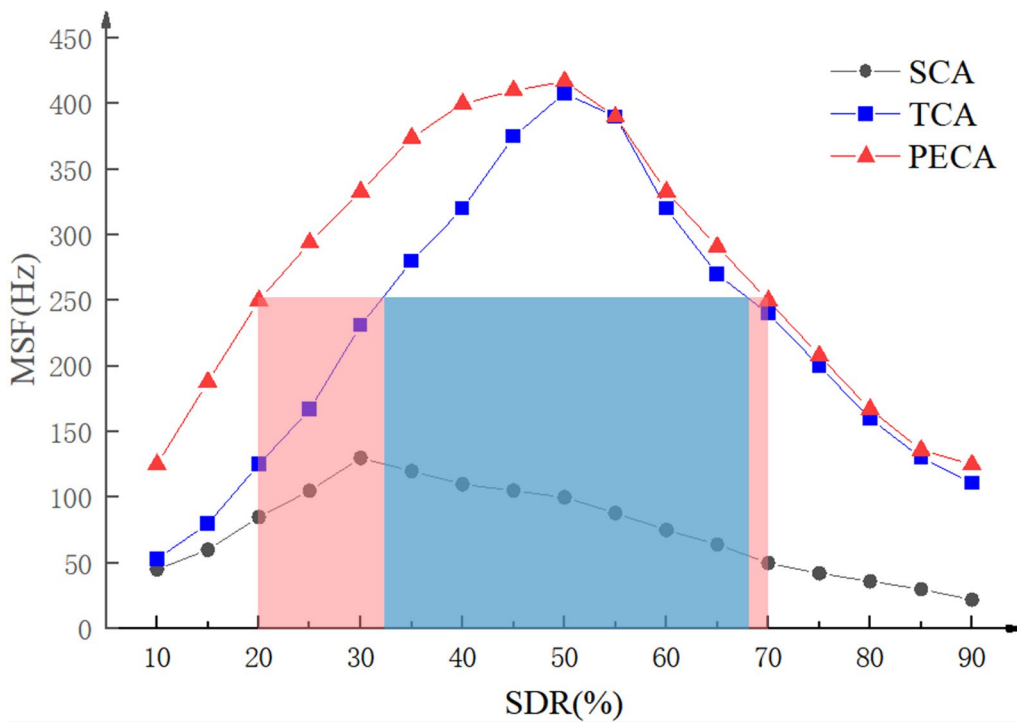

Figure 12 MSF results in overall SDR situation

necessary time to achieve complete closing of HSV. As a result, the further improvement of MSF is suppressed.

Taking into account the sufficient optimization condition (60% to 90% SDR), PECA has demonstrated a significant improvement in MSF, with an increase of nearly 300% compared to SCA. This result highlights the superiority of pre-excitation control.

4.3 Overall SDR Situation

This paper gets the MSF of HSV in SDR global domain and summarizes them, as shown in Figure 12.

The MSF obtained by HSV varies depending on the control algorithm employed. It is evident that the necessary time for opening and closing driven by SCA are respectively 2.31 ms and 4.2 ms. Based on Figure 6 and Eq. (21), the limit MSF should be taken at a SDR of around 35%. Similarly, it is inferred that PECA can achieve its limit MSF at a SDR of 51%. Based on the experimental results of MSF under different control algorithms in the overall SDR situation, it is found that when adopting a more effective control algorithm (PECA), the MSF of HSV can reach 417 Hz at approximately 50% SDR. In contrast, the limit MSF of HSV driven by SCA is around 130 Hz when the SDR is 30%. This difference can be attributed to the optimization of HSV's dynamic performance achieved through the pre-opening stage ①, pre-closing stage ③, and the closing stage ④ with a reverse high voltage in PECA. The main objective of the pre-opening stage ① and pre-closing stage ③ is to reduce the switching delay time. The closing stage ④ plays a crucial role in reducing both the closing delay time and the closing moving time. As a result, this optimization leads to excellent experimental results of FRC.

Additionally, the HSV does not operate at the limiting frequency, but adjusts the SDR within a certain range. A wider range of SDR adjustment has a more practical control effect at the same operating frequency. When analyzing the SDR in Figure 12 under 250 Hz frequency response condition, it is observed that the adjustable SDR range of PECA is from 20% to 70%, which has increased by approximately 14% compared to TCA's range of 32% to 68%. This optimization effect is attributed to the optimization effect of the pre-opening stage ①.

5 Conclusions

This paper investigates a pre-excitation control algorithm that achieves higher frequency response and wider SDR range adjustment of HSV through pre-excitation technology. The FRC experiment demonstrates that PECA effectively reduces the opening delay time, improves the controllable SDR and MSF without increasing the driving voltage. However, it should be noted that the MSF of HSV does not exhibit a completely linear relationship with the SDR. In higher frequency operating conditions, the increase in MSF will be somewhat limited.

(1) Optimizing the delay time can further enhance the MSF of HSV while maintaining its original dynamic performance. However, it is important to note that the increase in MSF is limited by the minimum opening and closing time, and the MSF does not exhibit a strictly linear relationship with the SDR.

(2) The MSF of PECA at each SDR is higher compared to that of SCA. Additionally, in certain small SDR operating conditions (10%−45%), the average frequency is higher than that of TCA, with an increase of approximately 93 Hz. The adjustable SDR range of PECA is also superior to the TCA at each frequency due to the effect of the pre-opening stage ①, showing an increase of about 14% under 250 Hz operating conditions.

(3) A higher frequency response of HSV signifies a smaller controllable SDR range. To obtain a higher switching frequency, it is advisable for the HSV control system to avoid operating in smaller or larger SDR conditions as much as possible, thereby achieving faster response speed and better control accuracy.

Declarations

References
[1] J Ruan, R Burton, P Ukratnetz. An investigation into the characteristics of a two dimensional "2D" flow control valve. *Journal of Dynamic Systems, Measurement and Control, Transactions of the ASME*, 2002, 124(1): 214-220.
[2] M Linjama, A Laamanen, M Vilenius. Is it time for digital hydraulics. *The Eighth Scandinavian International Conference on Fluid Power*, Tampere, Finland, May 7–9, 2003: 347-366.
[3] H Y Yang, M Pan. Engineering research in fluid power: A review. *Journal of Zhejiang University, Science A*, 2015, 16(6): 427-442.
[4] B Meng, H Xu, J Ruan, et al. Theoretical and experimental investigation on novel 2D maglev servo proportional valve. *Chinese Journal of Aeronautics*, 2021, 34(4): 416-431.

[5] Q Zhong, E G Xu, G Xie, et al. Dynamic performance and temperature rising characteristic of a high-speed on/off valve based on pre-excitation control algorithm. *Chinese Journal of Aeronautics,* 2023, 36(10): 445-458.

[6] B Meng, M Dai, C Zhu, et al. Analytical modelling and experiment of novel rotary electro-mechanical converter with negative feedback mechanism for 2D valve. *Chinese Journal of Mechanical Engineering*, 2022, 35: 122.

[7] H Wang, Z Chen, J Huang, et al. Development of high-speed on–off valves and their applications. *Chinese Journal of Mechanical Engineering*, 2022, 35: 67.

[8] L Chen, B Zhu, X D Sun, et al. Optimal allocation strategy for multi-motor drive system based on model predictive control. *Transactions of the Chinese Society for Agricultural Machinery*, 2018, 49(10): 403-409. (in Chinese)

[9] J S Zhao, C B Zhang, Z N Zhao, et al. Static and dynamic characteristics of high-speed on-off digital valves. *China Mechanical Engineering*, 2018, 29(2): 145-150.

[10] C Zhou, J Li, J Duan, et al. Control and jetting characteristics of an innovative jet valve with zoom mechanism and opening electromagnetic drive. *IEEE/ASME Transactions on Mechatronics*, 2015, 21(2): 1185-1188.

[11] I Y Lee. Switching response improvement of a high speed on/off solenoid valve by using a 3 power source type valve driving circuit. *2006 IEEE International Conference on Industrial Technology*, IEEE, 2006: 1823–1828.

[12] Q Zhong, B Zhang, H Y Yang, et al. Performance analysis of a high-speed on/off valve based on an intelligent pulse-width modulation control. *Advances in Mechanical Engineering*, 2017, 9(11): 1687814017733247.

[13] B Zhang, Q Zhong, J Ma, et al. Self-correcting PWM control for dynamic performance preservation in high speed on/off valve. *Mechatronics*, 2018, 55: 141-150.

[14] Q Gao, Y Zhu, Z Luo, et al. Analysis and optimization on compound PWM control strategy of high-speed on/off valve. *Journal of Beijing University of Aeronautics and Astronautics*, 2019, 45(6): 1129-1136.

[15] S V Angadi, R L Jackson, S Y Choe, et al. Reliability and life study of hydraulic solenoid valve-part 1: A multi-physics fifinite element model. *Engineering Failure Analysis*, 2009, 16(3): 874–887.

[16] S V Angadi, R L Jackson, S Y Choe, et al. Reliability and life study of hydraulic solenoid valve part2: Experimental study. *Engineering Failure Analysis*, 2009, 16(3): 944–963.

[17] J H Zhao, P F Yue, L Grekhov, et al. Hold current effects on the power losses of high-speed solenoid valve for common-rail injector. *Applied Thermal Engineering*, 2018, 128: 1579-1587.

[18] S N Cai, Y Jiao, C T Xu, et al. Energy-saving driver circuit of high-speed solenoid valve based on soft-switch technology. *2012 Second International Conference on Instrumentation, Measurement, Computer, Communication and Control, IEEE*, 2012: 598–601.

[19] X L Wang. *Research on electromagnetic driving energy consumption and temperature field characteristics of high speed on/off valve.* Hangzhou: Zhejiang University of Technology, 2022.

[20] J Zhao, M Wang, Z Wang, et al. Different boost voltage effects on the dynamic response and energy losses of high-speed solenoid valves. *Applied Thermal Engineering*, 2017, 123: 1494-1503.

[21] F Breidi, T Helmus, M Holland, et al. The impact of peak-and-hold and reverse current driving strategies on the dynamic performance of commercial cartridge valves. *Fluid Power Motion Control*, 2014. https://doi.org/10.1115/FPMC2014-7846.

[22] Q Zhong, X L Wang, G Xie, et al. Analysis of dynamic characteristics and power losses of high speed on/off valve with pre-existing control algorithm. *Energies*, 2021, 14(16): 4901.

[23] Z Liu, L Li, D Yue, et al. Dynamic performance improvement of solenoid screw-in cartridge valve using a new hybrid voltage control. *Machines*, 2022, 10(2): 106.

[24] Q Zhong, X L Wang, H Zhou, et al. Investigation into the adjustable dynamic characteristic of the high-speed on/off valve with an advanced pulsewidth modulation control algorithm. *IEEE/ASME Transactions on Mechatronics*, 2021, 27(5): 3784-3797.

[25] X Wang, F Y Hou. Control of brushless DC motor based on improved PSO-BP neural network. *Electronic Measurement Technology*, 2017, 40(2): 10-14. (in Chinese)

Qi Zhong   received his PhD degree from *Zhejiang University, China*, in 2019. He is now a distinguished professor at *Zhejiang University of Technology, China*.

Xiaotian Li   is currently a graduate student at *Zhejiang University of Technology, China*.

Yongxin Mao   is currently a graduate student at *Zhejiang University of Technology, China*.

Enguang Xu   is currently a graduate student at *Zhejiang University of Technology, China*.

Tiwei Jia   is currently a graduate student at *Zhejiang University of Technology, China*.

Yanbiao Li   is currently a professor at *Zhejiang University of Technology, China*.

Huayong Yang   is currently a professor at *Zhejiang University, China*. He has been a member of *Chinese Academy of Engineering* since 2013.